Spectrochimica Acta Part A: Molecular and Biomolecular Spectroscopy 147 (2015) 193–199

Contents lists available at ScienceDirect

Spectrochimica Acta Part A: Molecular and Biomolecular Spectroscopy

journal homepage: www.elsevier.com/locate/saa

Quantum chemical study on surface complex structures of phosphate on gibbsite

Carina V. Luengo [a,b,*], Norberto J. Castellani [b], Ricardo M. Ferullo [a]

[a] INQUISUR – Departamento de Química, Universidad Nacional del Sur, Bahía Blanca, Argentina
[b] Grupo de Materiales y Sistemas Catalíticos, Departamento de Física, Universidad Nacional del Sur, Bahía Blanca, Argentina

HIGHLIGHTS

- DFT calculations were used to identify phosphate surface complexes on gibbsite.
- Adsorption processes was simulated at two different pHs.
- Adsorption reactions were modelled via ligand exchange.
- ATR-FTIR spectra were obtained by subtracting to those containing only gibbsite.
- Surface complexes are thermodynamically more favored at acid pH.

GRAPHICAL ABSTRACT

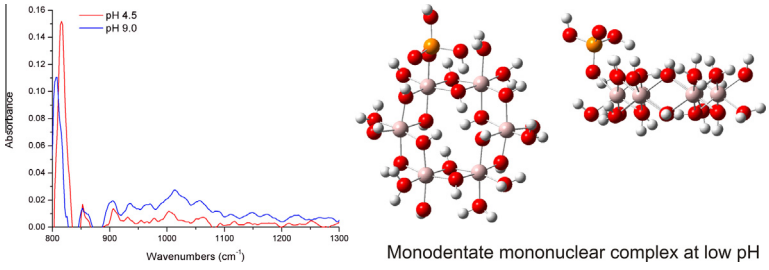

ARTICLE INFO

Article history:
Received 16 October 2014
Received in revised form 24 February 2015
Accepted 1 March 2015
Available online 9 March 2015

Keywords:
Gibbsite
Phosphate
DFT
Adsorption
ATR-FTIR

ABSTRACT

Quantum mechanics calculations based on the density functional theory (DFT) were used to identify phosphate surface complexes on gibbsite at low and high pH. The different phosphate species were represented using the $Al_6(OH)_{18}(H_2O)_6$ cluster model considering four different geometries: monodentate mononuclear (Pmm), monodentate binuclear (Pmb), bidentate mononuclear (Pbm) and bidentate binuclear (Pbb). The corresponding adsorption reactions were modelled via ligand exchange between phosphate species and surface functional groups (hydroxyls and protonated hydroxyls at high and low pH, respectively). The theoretical results indicate that phosphate surface complexes are thermodynamically more favored at acid pH, in agreement with experimental evidences. The first step in these reactions, i.e., the generation of required aluminum vacant sites, was predicted to be particularly favorable when singly coordinated aquo groups are released. Stretching and bending vibrational frequencies associated with the different surface structures were calculated at both pH conditions. The corresponding values at low pH were found to be shifted to higher frequencies with respect to those ones at high pH. ATR-FTIR studies were also carried out. The resulting spectra are dominated by a strong band within the 800–840 cm^{-1} interval due to $P–O_H$ stretching modes. The corresponding peak appearing around 820 cm^{-1} at high pH is shifted to lower frequencies with respect to the position at low pH, a tendency well predicted by DFT calculations.

Introduction

The presence of chemical contaminants in surface water and groundwater is an important problem in environmental chemistry. In particular, phosphate species has been recognized as one of the

* Corresponding author at: Departamento de Química, Universidad Nacional del Sur, Av. Alem 1253, 8000 Bahía Blanca, Argentina. Tel.: +54 291 4595101x3593; fax: +54 291 4595160.
E-mail address: cluengo@uns.edu.ar (C.V. Luengo).

http://dx.doi.org/10.1016/j.saa.2015.03.013
1386-1425/

main nutrients that controls eutrophication in surface water bodies [1–3]. Metal oxides (embracing with this expression those materials composed by the corresponding metal with O and/or OH) present in soils are efficient adsorbents and therefore they play an important role in regulating the bioavailability and mobility of anions [4].

Gibbsite is an aluminum hydroxide with high surface area and constitutes an important adsorbent of anions [5]. In the past, several experimental investigations have been performed on the adsorption of phosphate on gibbsite and other aluminum oxides [6–20]. Nevertheless, spectroscopic studies on these systems are not abundant in the literature [17,18]. In principle, the use of spectroscopic techniques provides very useful information on the identity of surface species that phosphate forms when it is adsorbed at the oxide–water interface. Particularly, vibrational frequencies active in IR are highly sensitive to the geometrical structure, protonation state and anion coordination environment, and thus, they provide an excellent tool to determine the composition and structure of adsorbed anions. In practice, however, there are many difficulties in assigning the absorption bands of vibrational spectra and to extract from them information related to the molecular structure of surface complexes. The scarce information on IR studies of phosphate adsorption on aluminum oxides, e.g., gibbsite and boehmite, is in part due to the superposition of IR absorption bands from the substrate and those arising from P–O stretching.

On the other hand, theoretical calculations are routinely used as an indispensable tool in chemical research. Theoretical modeling of adsorption processes on mineral surfaces has received much attention in recent decades. The availability of faster computers and the breakthrough of theoretical methods have allowed calculating more complex systems with remarkable accuracy. Quantum chemical simulations have been widely used to study surface complexes and they are very useful to help the interpretation of experimental measurements and to formulate hypotheses. In these studies, cluster models with a finite number of substrate atoms were usually used to represent the surface, by considering that the adsorption of a molecule is in general a localized phenomenon [21–27]. Such simple models can provide important insights into the structure of the specific adsorption complex. It has been shown that even relatively small clusters are sufficient to describe distances and bond angles of adsorbed molecules [22,25,28].

There is relatively scant information in the specialized literature about theoretical calculations describing the interaction of gibbsite surface with different solutes [28–33]. Therefore, there is still a great need for reliable quantum chemical investigations to study the structure and relative stability of different surface complexes, in particular concerning the activity of different adsorption surface sites. The structural environment of oxyanions on solid surfaces is in direct relation with its stability and remobilization. An important question is how such differences in the ligand structure can influence the adsorption reactions, in particular the binding mechanisms between the ligand and the surface. Following these motivations, in this work a quantum chemical analysis was performed to identify the dominant phosphate surface complexes on gibbsite. On the other hand, ATR-FTIR spectra were also obtained. At our knowledge, up to now this technique has not been used to study the phosphate–gibbsite interface.

Computational and experimental methods

Density functional calculations

Density functional theory (DFT) calculations were performed using the gradient corrected Becke's three parameters hybrid exchange functional in combination with the correlation functional of Lee, Yang and Parr (B3LYP) [34,35]. All the calculations were carried out using the Gaussian03 program package [36]. A basic cluster with the $Al_6(OH)_{18}(H_2O)_6$ formula was employed to represent the local structure of the gibbsite surface (Fig. 1). The surface geometry was obtained from crystallographic data [37,38]. In order to keep the cluster neutrality some hydroxyl groups monocoordinated to Al were replaced by H_2O [29]. Internal coordinates were used in the optimization procedure. Distances, bond angles and dihedral angles connecting Al atoms and bridged O atoms of the bottom part of the cluster were fixed at the crystallographic structure values. All the other parameters were fully optimized. The 6-311++G** basis set was employed for all the atoms.

The solvation of surface and solute has an important role in the adsorption process and it has to be taken into account in calculating optimized structures and adsorption reaction energies. The solvent effect has been evaluated using the polarizable continuum method (PCM) [39]. In all the cases the PCM technique was applied to both the optimization procedure and the calculation of the vibrational frequencies. The adsorption of phosphate was studied by using two different clusters, which represent the gibbsite surface at low and high pHs (see below). The different inner-sphere surface complexes of phosphate were adsorbed considering four different geometrical forms: monodentate mononuclear (Pmm), monodentate binuclear (Pmb), bidentate mononuclear (Pbm) and bidentate binuclear (Pbb). Vibrational frequencies have been computed by determining the second derivate of the total energy with respect to the internal coordinates. The calculated vibrational modes were visualized using the GaussView program [40].

ATR-FTIR spectroscopy

Adsorption of phosphate on gibbsite was monitored by ATR-FTIR (Attenuated total reflectance Fourier transform infrared) spectroscopy with a ZnSe crystal. For the present work, gibbsite manufactured by BDH Chemicals was used. The solid was characterized by a set of different techniques such as IR spectroscopy, XRD (X-ray diffraction), SEM (scanning electron microscopy), EDX (Energy-dispersive X-ray spectroscopy), XRF (X-ray fluorescence), DTA (Differential thermal analysis) and TGA (Thermogravimetric analysis).

The adsorption of phosphate on gibbsite was carried out in several plastic tubes at pH values of 4.5 and 9.0. For that purpose, 100 mg of solid gibbsite and 20 mL of 0.1 M KCl solution were introduced to each tube. Then, different volumes of a 1×10^{-3}M KH_2PO_4 solution were incorporated to the reaction tubes. Additional experiments were performed in absence of the phosphate solution. The pH of the resulting dispersion was then adjusted to the desired value by adding HCl or KOH solutions. This time was set as the initial time of the adsorption reaction.

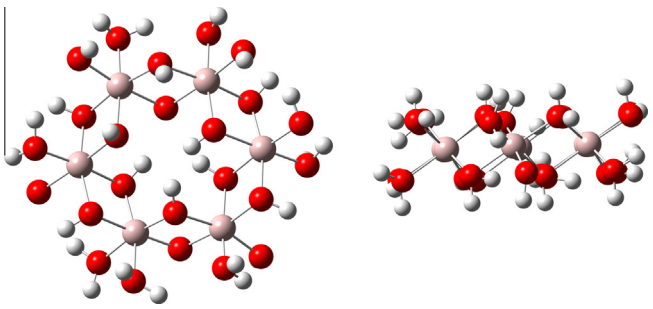

Fig. 1. $Al_6(OH)_{18}(H_2O)_6$ cluster model representing the gibbsite surface. Left panel: top view. Right panel: side view. Red balls: oxygen; pink balls: aluminum; small white balls: hydrogen. (For interpretation of the references to colour in this figure legend, the reader is referred to the web version of this article.)

The reaction temperature was the room temperature (~25 °C). The mixture of the dispersion was done by a Vicking rotary shaker. The adsorption reaction was followed for 5 h and the pH was continuously checked and kept constant by adding small volumes of concentrated HCl or KOH solutions. After 5 h, the tubes were centrifuged at 5000 rpm during 10 min and the supernatant extracted. In all the experiments, the pH was measured with a Crison GLP 22 pH meter and a Radiometer GH2401 combined pH electrode.

The resulting solid of each tube was resuspended with a 0.1 M KCl solution, to the desired pH value, either 4.5 or 9.0. The so obtained dispersions were monitored by ATR-FTIR spectroscopy. Previously, the ZnSe crystal was covered with a 0.1 M KCl solution and a blank spectrum was recorded in the 400–4000 cm^{-1} wavenumber range. After this, the electrolyte solution was withdrawn and the gibbsite dispersions, either at pH 4.5 or 9.0, were added and the spectra were then recorded. The ZnSe crystal was cleaned after each measurement by washing with water.

The experiments were performed with a Nicolet Magna 560 FTIR instrument equipped with a DTGS detector. Each spectrum is the result of 256 co-added interferograms. The spectral resolution was 4 cm^{-1} in all cases, and the working temperature was 25 ± 2 °C. To obtain the spectra of adsorbed phosphate species, the spectra of tubes containing phosphate and gibbsite was subtracted to those containing only gibbsite.

Results and discussion

Preliminary results

In order to define the predominant adsorbed phosphate species that are present on gibbsite a preliminary experimental search was carried out. The corresponding phosphate species distribution is shown in the Supplementary material (Fig. S1). At low pH, between 4 and 6, the $H_2PO_4^-$ species is predominant whereas at high pH, between 9 and 11, the HPO_4^{2-} species is the most important. This distribution was obtained using the MINEQL program [41]. The pKa values of phosphoric acid are 2.12, 7.21 and 12.67.

The PZC (point zero charge) values for gibbsite have been determined by various techniques, including acid–base titration, potentiometric titration, microelectrophoresis, and salt titration. The PZC of a solid suspension is the pH value at which the solid surface has neutral net charge. For pH values bellow this PZC the surface is net positively charged, and for pH values above the corresponding PZC the surface is net negatively charged [4]. The PZC values reported in literature for gibbsite are in the range of 7.8–10.0 with an average value of 9.0 [42,43]. This information was used to simulate the charge of the cluster, as we shall see later.

Free phosphate

Free $H_2PO_4^-$ and HPO_4^{2-} phosphate species were fully optimized using the 6-311++G** basis set. The ATR-FTIR spectra of free phosphate in aqueous solution at different pHs are shown in Fig. 2 (inset). Data analysis is focused in the 800–1300 cm^{-1} region where bands associated with various phosphate vibration modes are found. Experimental and calculated frequencies are summarized in Table 1. The assignment of IR absorption bands is in agreement with other works [44–46].

Adsorbed phosphate on gibbsite

Taking into account the results shown in Preliminary results, the low pH conditions were simulated in our DFT calculations by adsorbing the $H_2PO_4^-$ species on a positive charged gibbsite, while the high pH conditions were modelled by anchoring the HPO_4^{2-} species on a neutral gibbsite surface.

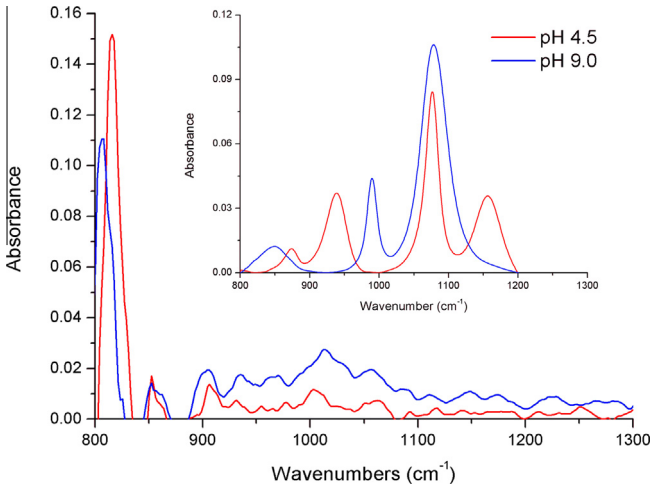

Fig. 2. ATR-FTIR spectra of phosphate adsorbed on gibbsite at pH 4.5 and 9.0. Inset: ATR-FTIR spectra of free phosphate in aqueous solution at pH 4.5 and 9.0.

Table 1
Calculated and experimental IR vibrational frequencies (in cm^{-1}) for free phosphate in aqueous solution.

Calculated	Experimental	Assignment
$H_2PO_4^-$		
747		ν_s P–O_H
764	874	ν_{as} P–O_H
993	940	δ_{as} POH
1030		δ_s POH
1054	1075	ν_s P–O
1236	1155	ν_{as} P–O
HPO_4^{-2}		
647		ν P–O_H
924	847	ν_s P–O
992	989	δ POH
1045		ν_{as} P–O
1081	1077	ν_{as} P–O

The different adsorbed species of phosphate were optimized at both high and low pH. The optimized structures are shown in Fig. 3. To simulate the surface at low pH the $[Al_6(OH)_{17}(H_2O)_6(OH_2)]^+$ cluster was used, in which one surface hydroxyl close to the adsorption site is protonated. For obtaining Pmm and Pbb complexes, one and two monocoordinated OH^- groups are released, respectively (for Pbb, belonging to two different Al centers). On the other hand, the Pmb structure was constructed by eliminating one bridged hydroxyl. Note that at low pH, starting from the Pbm geometry as input, another Pmb complex can be obtained, indicated from now on as Pmb*; in this case, one of the Al adjacent sites remains unsaturated. To model Pbm (high pH) and Pmb* (low pH) complexes, one singly coordinated and one bridged hydroxyl groups are simultaneously released.

Because of the similarity between P(V) and As(V) oxoanions and the lack of EXAFS studies for the former species on gibbsite, available EXAFS analysis of As(V) on gibbsite can be used for comparison [28], especially taking into account that atomic and ionic radii of P are only 0.1–0.15 Å shorter than those of As. This EXAFS study was carried out in solutions of pH of 5.5 in which $H_2AsO_4^-$ is the predominant species. The P-Al distance is predicted by our DFT calculations to be 3.10–3.30 Å for both monodentate and bidentate species, both at low pH. The experimental average value of the As–Al distance determined by EXAFS is 3.19 Å. Another geometrical parameter that can be compared directly with

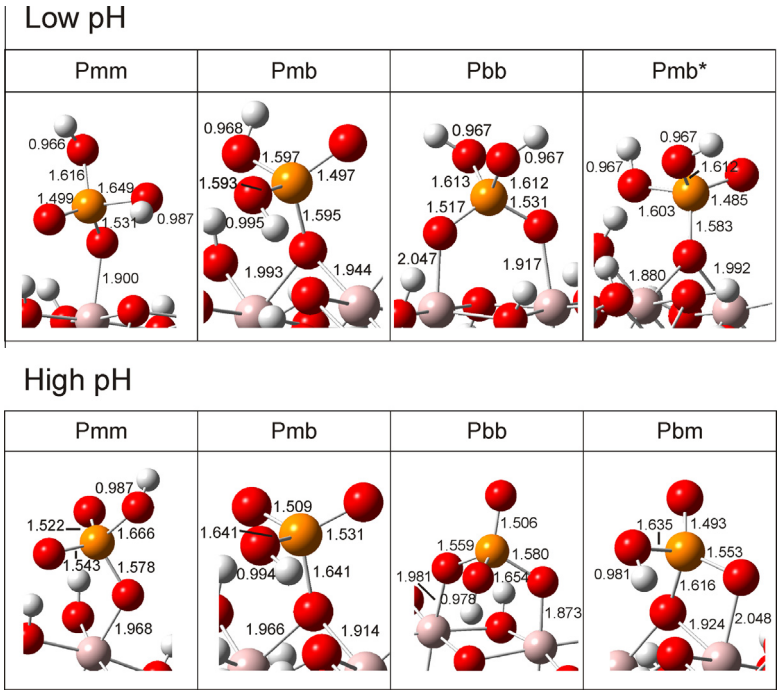

Fig. 3. Optimized structures of adsorbed species of phosphate at low and high pH.

the EXAFS results is the As–O bond distance, estimated to be of 1.68 Å in average, while our DFT calculations, at low pH, predict P–O distances of 1.48–1.65 Å for monodentate and 1.52–1.61 Å for bidentate species.

ATR-FTIR spectra of phosphate adsorbed on gibbsite at pH 4.5 and 9.0 are shown in Fig. 2 (clearer spectra in the 800–1300 cm^{-1} region are presented in the Supplementary material Fig. S2). These spectra were obtained from the difference between the spectra of gibbsite with and without phosphate. Owing to the surface complexity of the gibbsite sample, surface phosphates are expected to present a wide variety of adsorption modes. For this reason, the IR spectra of Fig. 2 are not simple and performing an unequivocal assignment of all the bands results a very difficult task.

Now we examine the calculated vibrational frequencies associated with different surface structures. The assignment of the bands predicted by our theoretical models is presented in Tables 2 and 3. For simplicity, we did not distinguish between symmetric and asymmetric modes. All the adsorption modes, at both pH conditions, present several frequency values approximately between 800 and 1250 cm^{-1}. In the last column of Tables 2 and 3, the position of the main intensive bands observed from the IR spectra was added.

Table 2
Frequency values (in cm^{-1}) calculated at low pH. The positions of some relevant peaks of the ATR-FTIR spectrum is also shown (obtained from Fig. 2).

Pmm	Pmb	Pbb	Pmb*	Assignment	Exp.
849	850	829	835	νP–O_H	821, 853,
	902[b]	873	875		906, 930
	919		950[a]		977
1001[a]		990[a], 1017[a]		δPOH	1003
	1044		1032		1063
1062[b]		1073[b]	1039[b]	νP–O_{Al}	
		1157			
1201[b]	1190[b]		1237	νP–O	
1230	1250			δPOH	

[a] Combined with P–O_{Al} stretching.
[b] Combined with POH bending.

Table 3
Frequency values (in cm^{-1}) calculated at high pH. The positions of some relevant peaks of the ATR-FTIR spectrum is also shown (obtained from Fig. 2).

Pmm	Pmb	Pbb	Pbm	Assignment	Exp.
765[b]	794, 814	772	807	νP–O_H	810
	860[b]			νP–O_{Al}	852
914[a]		924	909		905, 928
1006[a]		980	975		970
	1021[a]			δPOH	1013, 1057
1106[b]		1123[b]		νP–O	1150
			1162[a]	δPOH	1174
	1157[b]			νP–O	1225
	1269	1215[b]	1252[b]		
1271				δPOH	

[a] Combined with PO stretching.
[b] Combined with POH bending.

As expected, differences in the bond length reflect changes in the vibrational frequencies. Elongated bonds, and therefore weak bonds, correspond to low vibrational frequencies, and vice versa. In general, for the different surface complexes and at both pH, the distance of P–O_H bond is longer than that of P–O_{Al}. This is because hydrogen withdraws more electronic charge from the O than the metal does [47]. Therefore, the bond strength of P–O_H is weaker than that of P–O_{Al}, which is consistent with the lower P–O_H frequencies than those of P–O_{Al}. On the other hand, the P–O bond strength is the strongest of among all the bonds between P and O, and therefore, this group presents the highest vibrational frequency (around 1200 cm^{-1}).

We can observe that for each type of stretching mode, the corresponding calculated values at high pH become shifted to lower frequencies with respect to the values at low pH. For instance, the vibrational frequencies of P–O_{Al} at high pH appear around 860–1010 cm^{-1}, and in the range of 1040–1160 cm^{-1} at low pH. This effect can be due to the presence of an additional P–O group at high pH, which produces a lower strength of the P–O_{Al} bond by withdrawing electronic charge from this covalent bond. The same situation occurs with the frequency of the P–O_H

bonds, appearing at lower frequency for high pH (specifically at 760–810 cm^{-1} for high pH and at 830–900 cm^{-1} for low pH); as before, this can be produced by the additional P–O group at high pH which weakens the P–O_H bond. On the other hand, the stretching modes of P–O bonds are located above 1190 cm^{-1} at low pH, and above 1160 cm^{-1} at high pH. The relative positions of the bands are in qualitative agreement with that reported by Guan et al. [17], Tejedor-Tejedor and Anderson [46], Kwon and Kubicki [47], Arai and Sparks [48] and Zenobi et al. [49].

We note that in the ATR-FTIR spectra two sharp bands at 800–840 cm^{-1} are clearly observed, very likely due to P–O_H stretching modes. At high pH the strong band at about 820 cm^{-1} is shifted to lower frequencies with respect to the position at low pH. As discussed above, this is in line with our theoretical findings. According to the theoretical results, and in general terms considering both pH conditions, the bands detected in the spectra within the 900–1080 cm^{-1} interval could correspond to P–O_{Al} stretching and POH bending modes mainly, and to P–O stretching for the peaks above 1100 cm^{-1}.

Regarding the adsorption reactions, as a first approximation we can postulate that they occur by exchanging one or two hydroxyl groups (the leaving species) for phosphate species (the incoming species). According to the corresponding optimized structures, the reactions are:

Low pH:

$$\text{Pmm, Pmb}: \ H_2PO_4^- + G^+ \rightarrow [H_2PO_4{-}G]^+ + OH^- \quad (1)$$

$$\text{Pbb,Pmb}^*: H_2PO_4^- + G^+ \rightarrow [H_2PO_4{-}G]^{+2} + 2OH^- \quad (2)$$

High pH:

$$\text{Pmm, Pmb}: \ HPO_4^{2-} + G^0 \rightarrow [HPO_4{-}G]^- + OH^- \quad (3)$$

$$\text{Pbb, Pbm}: \ HPO_4^{2-} + G^0 \rightarrow [HPO_4{-}G]^0 + 2OH^- \quad (4)$$

In Eqs. (1)–(4) "G^0" and "G^+" indicate the above-mentioned gibbsite clusters, i.e., $[Al_6(OH)_{18}(H_2O)_6]^0$ and $[Al_6(OH)_{17}(H_2O)_6(OH_2)]^+$, respectively.

The energies for the reaction between the phosphate species and the gibbsite surface in solution, according to reactions (1)–(4), were calculated as the difference between the total energy of the products and that of the reactants. The corresponding values are summarized in Table 4.

All the reactions between phosphate species and gibbsite resulted to be endothermic. Furthermore, at both pH conditions, the reaction energy values suggest that monodentate complexes are more likely to be formed on gibbsite, compared with bidentate complexes.

Reactions (1)–(4) can be considered to occur in two steps. In the first step, endothermic, one or two OH^- groups are eliminated, producing the required unsaturated Al sites. In the second step, exothermic, the phosphate species are trapped and strongly anchored to the surface. For example, at low pH and for the monodentate complex (reaction (1)) these two steps are:

$$\text{Step 1}: \ G^+ \rightarrow G^{2+*} + OH^- \quad (5)$$

$$\text{Step 2}: \ H_2PO_4^- + G^{2+*} \rightarrow [H_2PO_4{-}G]^+ \quad (6)$$

Table 4
Calculated reaction energies (in kJ/mol) of phosphate on gibbsite in aqueous solution, modelled by hydroxyl-phosphate exchange.

Low pH		High pH	
Pmm	44	Pmm	9
Pmb	65	Pmb	23
Pbb	193	Pbb	91
Pmb*	298	Pbm	171

In these equations, "G^{2+*}" indicates the gibbsite surface with one unsaturated Al site and corresponds to the $[Al_6(OH)_{16}(H_2O)_6(OH_2)]^+$ cluster. Similar reactions for the other cases can be formulated.

The energies associated with the first step, i.e., the one that implies the releasing of one or two OH^-, at low pH, are 164, 408, 400 and 651 kJ/mol for Pmm, Pmb, Pbb and Pmb*, respectively. On the other hand, the corresponding values at high pH are somewhat smaller: 136, 382, 377 and 577 kJ/mol for Pmm, Pmb, Pbb and Pbm, respectively. These results indicate a greater tendency to generate the required vacancies at high pH. Besides, the energies for global reactions reported in Table 4 also indicate that each type of surface complex is thermodynamically more favored at basic pH than at acid pH. However, this prediction is in disagreement with experiments. Indeed, it was previously shown that the amount of phosphate adsorbed on gibbsite decreases as pH increases [7,14,50]. Studies using IR and ^{31}P solid-state NMR measurements have indicated that phosphate is sorbed by a combination of surface complexation and surface precipitation, with the relative amounts of these phases depending on pH and phosphate concentration [7,8,16,18,51]. At low pH and high phosphate concentrations, sorption is dominated by the presence of both amorphous and crystalline precipitate phases. On the other hand, Laiti et al. [18] also found that both an increasing in the phosphate concentration and a decreasing in pH, increases the fraction of the precipitate phase.

In light of these results, an alternative modeling for low pH can be proposed, as discussed by Paul et al. [24]. It was previously suggested [19] that the increase in the amount of adsorbed phosphate at low pH can be attributable to the relative facility to release OH^- groups. Indeed, the protonation of the leaving OH^- group can weaken the Al–O bond and facilitate the removal of OH^- as H_2O. In this way the adsorption of phosphate species is favored when the amount of aquo sites, Al–OH_2^+, increases with decreasing pH. According to this mechanism, the following reactions can be proposed:

$$\text{Pmm, Pmb}: \ H_2PO_4^- + G^{2+} \rightarrow [H_2PO_4{-}G]^+ + H_2O \quad (7)$$

$$\text{Pbb, Pmb}^*: \ H_2PO_4^- + G^{3+} \rightarrow [H_2PO_4{-}G]^{+2} + 2H_2O \quad (8)$$

In these equations "G^{2+}" indicates that a second proton was added to the G^+ cluster of Eqs. 1 and 2. It corresponds to the $[Al_6(OH)_{16}(H_2O)_6(OH_2)_2]^{+2}$ cluster (Fig. 4). "G^{3+}" corresponds to the situation where two leaving OH^- are protonated and to the $[Al_6(OH)_{15}(H_2O)_6(OH_2)_3]^{+3}$ cluster model.

As in the previous model, the global adsorption reactions considered in Eqs. 7 and 8 can be viewed as constituted by two steps. The first one is the generation of vacant sites and it involves the removing of one or two aquo groups. The second one involves the anchorage of the phosphate species. For monodentate adsorption (Pmm and Pmb):

$$\text{Step 1}: \ G^{2+} \rightarrow G^{2+*} + H_2O \quad (9)$$

$$\text{Step 2}: \ H_2PO_4^- + G^{2+*} \rightarrow [H_2PO_4{-}G]^+ \quad (10)$$

Here, "G^{2+*}" corresponds to the gibbsite surface with the required Al vacancy and to the $[Al_6(OH)_{16}(H_2O)_6(OH_2)]^{+2}$ cluster model. For Pbb and Pmb* the corresponding steps are:

$$\text{Step 1}: \ G^{3+} \rightarrow G^{3+*} + 2H_2O \quad (11)$$

$$\text{Step 2}: \ H_2PO_4^- + G^{3+*} \rightarrow [H_2PO_4{-}G]^{2+} \quad (12)$$

In Fig. 4 the optimized structures for the protonated gibbsite surfaces are presented for all the complexes, together with the resulting active sites.

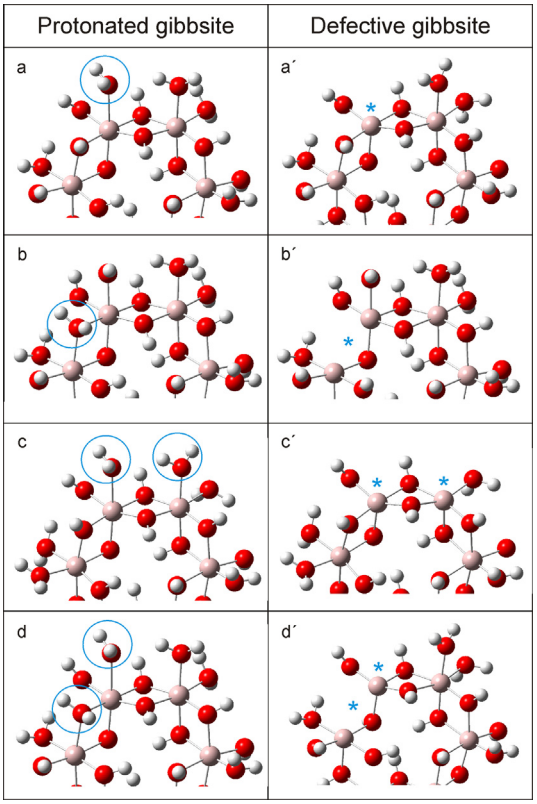

Fig. 4. Clusters used for modelling the reaction at low pH, considering the protonation of the leaving hydroxyl groups (marked by circles). Optimized structures of protonated gibbsite surfaces (left column) and the resulting surfaces with the corresponding active sites (marked by stars; right column): (a)–(a′) for Pmm; (b)–(b′) for Pmb; (c)–(c′) for Pbb; and (d)–(d′) for Pmb*.

In Table 5 the reaction energies for partial and global reactions are shown. Note that with this alternative mechanism the surface complexes are thermodynamically more favored at acid pH, in agreement with experiments. Besides, the global reactions resulted to be all exothermic. Clearly, the elimination of protonated OH^- is a more favorable process than the unprotonated one.

For all the cases, the rate-limiting step is the reaction corresponding to the generation of the vacant sites. In other words, in order to attain step 2, the generation of vacant sites is required firstly (step 1). It is apparent that the releasing of a singly coordinated aquo group, $Al–OH_2^+$, to generate Pmm should be a very favorable process (reaction energy of only 49 kJ/mol). For comparison, the energy to break the doubly coordinated aquo group, $Al{=}OH_2^+$, is 145 kJ/mol, because in this case two Al–O links must be broken to yield Pmb. It is interesting to note that this energy is essentially the same than that required to eliminate two singly coordinated OH^- (Pbb). For the last case schematized in Fig. 4, three Al–O bonds are broken, and because of that this process demands the largest amount of energy (216 kJ/mol). In view of these results, considering the high reaction rate to release singly coordinated hydroxyls, a large population of phosphates adsorbed in the Pmm manner is expected.

Table 5
Parcial and global reaction energies (in kJ/mol) of phosphate on gibbsite in aqueous solution at low pH, modelled by protonation of the leaving hydroxyl groups.

	Low pH		
	Step 1	Step 2	Global
Pmm	49	−120	−71
Pmb	145	−343	−198
Pbb	143	−207	−64
Pmb*	216	−353	−137

As mentioned, the Al–O bond weakens when the hydroxyl group is protonated in comparison with the unprotonated case, as reflected in the interatomic distances. The Al–O distance is 16% and 8% longer for singly coordinated $Al–OH_2^+$ (Fig. 4a) and doubly coordinated $Al{=}OH_2^+$ (Fig. 4b), respectively, in comparison with the corresponding unprotonated situations.

It is interesting to note that the energy required to eliminate hydroxyl groups (step 1) for all the complexes with this alternative model is about 2.7 times lower than that demanded for the same situation but at high pH.

NMR studies performed by Van Emmerik et al. [7] suggest that inner-sphere complexes are bound to the singly coordinated Al–OH sites probably as monodentate complexes. On the other hand, Laiti et al. [18] used FTIR spectroscopy to study the sorption of phosphate on alumina and proposed the initial formation of a monodentate inner-sphere complex. Their results indicated that this inner-sphere complex is the precursor to the formation of an $AlPO_4$ phase. At least in principle, these experimental observations are in line with the greater tendency to eliminate singly coordinated hydroxyl groups to yield Pmm complexes observed in our models.

Summary and conclusions

The reaction of phosphate species with the gibbsite surface was studied using quantum chemical calculations. Two different pH conditions were analyzed by modeling positively charged and neutral clusters, for low and high pH, respectively. The adsorption of predominant phosphate species experimentally observed, $H_2PO_4^-$ and HPO_4^{2-} at low and high pH, respectively, was simulated on the corresponding surfaces. The solvent effect was evaluated using the polarizable continuum method (PCM).

Vibrational modes of the different phosphate surface complexes were calculated at low and high pH. The results show that, for each type of stretching mode, the corresponding values at low pH are predicted to be shifted to higher frequencies with respect to those ones at high pH. For instance, the vibrational frequency of $P–O_{Al}$ appears in different regions: in the range of 1040–1150 cm^{-1} at low pH, and within the 850–1000 cm^{-1} interval at high pH.

The ATR-FTIR spectra are dominated by a strong band between 800 and 850 cm^{-1} due to $P–O_H$ stretching modes; the different positions of these peaks at low and high pH are qualitatively well predicted by calculations. This effect can be due to the presence of an additional P–O group in the complexes present at high pH, which weakens both the $P–O_{Al}$ and $P–O_H$ bonds by withdrawing electronic charge. In general terms, considering both pH conditions, simulations predict that the bands in the range of 900–1080 cm^{-1} detected in the ATR-FTIR spectra could correspond to $P–O_{Al}$ stretching and POH bending modes mainly; above 1100 cm^{-1}, the peaks could be attributable principally to P–O stretching modes.

The reaction with phosphate was modeled by the substitution of one or two surface hydroxyl groups of gibbsite, to yield monodentate or bidentate surface complexes. When the reactions are simulated by means of a simple exchange between OH^- and phosphate species, each type of surface complex becomes thermodynamically more favored at basic pH than at acid pH, in a clear disagreement with experimental evidences. However, an alternative modeling was also considered at low pH, consisting of the protonation of the leaving hydroxyl groups. This last model seems to describe properly the reactions occurring at low pH because it reproduces the correct tendency.

The first step in these reactions, i.e., the generation of the required aluminum vacant sites, is found to be highly favorable

for singly coordinated hydroxyl or aquo groups, so that Pmm geometry is predicted to be a favorable adsorption mode at both pH. The corresponding energy for the global reaction resulted to be exothermic for low pH, −71 kJ/mol, and slightly endothermic for high pH, 9 kJ/mol.

In summary, in this work we have tried to cover the lack of information at a fundamental level concerning the structure and stability of phosphate on gibbsite. For that purpose, optimized structures, reaction energies and frequencies were calculated. We have showed that quantum chemical calculations can provide insight into surface complex formation in a way that complements the experimental information.

Acknowledgments

This work was financed by CONICET, ANPCyT and SECyT-UNS. C.L. thanks CONICET for the posdoctoral fellowships.

Appendix A. Supplementary data

Supplementary data associated with this article can be found, in the online version, at http://dx.doi.org/10.1016/j.saa.2015.03.013.

References

[1] H. Klapper, Control of Eutrophication in Inland Water, Ellis Horwood, Chichester, 1991.
[2] V.H. Smith, Environ. Sci. Pollut. Res. 10 (2003) 126–139.
[3] Q. Zhou, C.E. Gibson, Y. Zhu, Chemosphere 42 (2001) 221–225.
[4] D.L. Sparks, Environmental Soil Chemistry, Elsevier Science, USA, 2003.
[5] S. Goldberg, J.A. Davis, J.D. Hem, in: G. Sposito (Ed.), The Environmental Chemistry of Aluminum, Lewis Publishers, New York, 1996, pp. 271–331.
[6] M. Kabayama, T. Sakiyama, N. Kawasaki, T. Nakamura, M. Araki, S. Tanada, J. Chem. Eng. Jpn. 36 (2003) 499–505.
[7] T.J. Van Emmerik, D.E. Sandström, O.N. Antzutkin, M.J. Angove, B.B. Johnson, Langmuir 23 (2007) 3205–3213.
[8] W.H. van Riemsdijk, J. Lyklema, J. Colloid Interface Sci. 76 (1980) 55–66.
[9] J.H. Kyle, A.M. Posner, J.P. Quirk, J. Soil Sci. 26 (1975) 32–43.
[10] S.S.S. Rajan, Nature 262 (1976) 45–46.
[11] R.L. Parfitt, A.R. Fraser, J.D. Russell, V.C. Farmer, J. Soil Sci. 28 (1977) 40–47.
[12] L. Lijklema, Environ. Sci. Technol. 14 (1980) 537–541.
[13] W.H. van Riemsdijk, F.A. Weststrate, G.H. Bolt, Nature 257 (1975) 473–474.
[14] D. Muljadi, A.M. Posner, J.P. Quirk, J. Soil Sci. 17 (1966) 212–228.
[15] D. Muljadi, A.M. Posner, J.P. Quirk, J. Soil Sci. 17 (1966) 230–237.
[16] W.H. van Riemsdijk, J. Lyklema, Colloids Surf. 1 (1980) 33–44.
[17] X.H. Guan, Q. Liu, G.H. Chen, C. Shang, J. Colloid Interface Sci. 289 (2005) 319–327.
[18] E. Laiti, P. Persson, L.O. Öhman, Langmuir 14 (1998) 825–831.
[19] X. Guan, G. Chen, C. Shang, J. Environ. Sci. 19 (2007) 312–318.
[20] D. Muljadi, A.M. Posner, J.P. Quirk, J. Soil Sci. 17 (1996) 238–247.
[21] L. Tribe, K.D. Kwon, C.C. Trout, J.D. Kubicki, Environ. Sci. Technol. 40 (2006) 3836–3841.
[22] D.M. Sherman, S.R. Randall, Geochim. Cosmochim. Acta 67 (2003) 4223–4230.
[23] S.C.B. Myneni, S.J. Traina, G.A. Waychunas, T.J. Logan, Geochim. Cosmochim. Acta 62 (1998) 3285–3300.
[24] K.W. Paul, J.D. Kubicki, D.L. Sparks, Environ. Sci. Technol. 40 (2006) 7717–7724.
[25] C.L. Peacock, D.M. Sherman, Geochim. Cosmochim. Acta 68 (2004) 2623–2637.
[26] Z. Wei, S. Zhang, Z. Pan, Yue Liu, Appl. Surf. Sci. 258 (2011) 1192–1198.
[27] Z. Lou, Q. Zeng, X. Chu, F. Yang, D. He, M. Yang, M. Xiang, X. Zhang, H. Fan, Appl. Surf. Sci. 258 (2012) 4911–4916.
[28] A.C.Q. Ladeira, V.S.T. Ciminelli, H.A. Duarte, M.C.M. Alves, A.Y. Ramos, Geochim. Cosmochim. Acta 65 (2001) 1211–1217.
[29] A.F. Oliveira, A.C.Q. Ladeira, V.S.T. Ciminelli, T. Heine, H.A. Duarte, J. Mol. Struct. Theochem. 762 (2006) 17–23.
[30] L. Favaro, A. Boumaza, P. Roy, J. Lédion, G. Sattonnay, J.B. Brubach, A.M. Huntz, R. Tétot, J. Solid State Chem. 183 (2010) 901–908.
[31] A.R. Ferreira, M.J.F. Martins, E. Konstantinova, R.B. Capaz, W.F. Souza, S.S.X. Chiaro, A.A. Leitão, J. Solid State Chem. 184 (2011) 1105–1111.
[32] T. Hattori, T. Saito, K. Ishida, A.C. Scheinost, T. Tsuneda, S. Nagasaki, S. Tanaka, Geochim. Cosmochim. Acta 73 (2009) 5975–5988.
[33] G. Duarte, V.S.T. Ciminelli, M.S.S. Dantas, H.A. Duarte, I.F. Vasconcelos, A.F. Oliveira, K. Osseo-Asare, Geochim. Cosmochim. Acta 83 (2012) 205–216.
[34] A.D. Becke, Phys. Rev. A 38 (1988) 3098–3100.
[35] C. Lee, W. Yang, R.G. Parr, Phys. Rev. B. 37 (1988) 785–798.
[36] M.J. Frisch et al., Gaussian 03, Revision C.02, Gaussian Inc., Wallingford, CT, 2004.
[37] H. Saalfeld, M. Wedde, Z. Krist. 139 (1974) 129–135.
[38] E. Balan, M. Lazzeri, G. Morin, F. Mauri, Am. Mineral. 91 (2006) 115–119.
[39] E. Cancès, B. Mennucci, J. Tomasi, J. Chem. Phys. 107 (1997) 3032–3041.
[40] M.J. Frisch et al., GaussView Reference, Gaussian Inc., Wallingford, CT, 2003.
[41] Westall J.C., Zachary J.L. y Morel F.M.M. 1976. MINEQL, A computer program for the calculation of chemical equilibrium composition of aqueous systems. Water Quality Laboratory, Ralph M. Parsons Laboratory for Water Resources and Environmental Engineering, Department of Civil Engineering, Massachusetts Institute of Technology, pp. 91.
[42] M. Kosmulski, Adv. Colloid Interface Sci. 152 (2009) 14–25.
[43] A.K. Karamalidis, D.A. Dzombak, Surface complexation modeling: gibbsite, John Wiley and Sons, New Jersey, 2010.
[44] M. Klähn, G. Mathias, C. Kotting, M. Nonella, J. Schlitter, K. Gerwert, P. Tavan, J. Phys. Chem. A 108 (2004) 6186–6194.
[45] C. Luengo, M. Brigante, J. Antelo, M. Avena, J. Colloid Interface Sci. 300 (2006) 511–518.
[46] M.I. Tejedor-Tejedor, M.A. Anderson, Langmuir 6 (1990) 602–611.
[47] K.D. Kwon, J.D. Kubicki, Langmuir 20 (2004) 9249–9254.
[48] Y. Arai, D.L. Sparks, J. Colloid Interface Sci. 241 (2001) 317–326.
[49] M.C. Zenobi, C.V. Luengo, M.J. Avena, E.H. Rueda, Spectrochim. Acta Part A Mol. Biomol. Spectrosc. 75 (2010) 1283–1288.
[50] A.J. Fitzpatrick, Adsorption of arsenate and phosphate on gibbsite from artificial seawater, McGill University, Canada, 1998.
[51] R. Lookman, P. Grobet, R. Merckx, W.H. van Riemsdijk, Geoderma 80 (1997) 369–388.